Available online at www.sciencedirect.com
ScienceDirect
Agricultural and Forest Meteorology 145 (2007) 48–68
AGRICULTURAL AND FOREST METEOROLOGY
www.elsevier.com/locate/agrformet

Modelling net ecosystem carbon and water exchange of a temperate *Eucalyptus delegatensis* forest using multiple constraints

Miko U.F. Kirschbaum [a,b,c,*], Heather Keith [b], Ray Leuning [a,d], Helen A. Cleugh [d], Kris L. Jacobsen [b], Eva van Gorsel [d], R. John Raison [a,e]

[a] *CRC for Greenhouse Accounting, GPO Box 475, Canberra, ACT 2601, Australia*
[b] *CSIRO Climate Program, GPO Box 3023, Canberra, ACT 2601, Australia*
[c] *Environmental Biology Group, RSBS, Australian National University, GPO Box 475, Canberra, ACT 2601, Australia*
[d] *CSIRO Marine and Atmospheric Research, GPO Box 1666, Canberra, ACT 2601, Australia*
[e] *Ensis, PO Box E4008, Kingston, ACT 2604, Australia*

Received 8 August 2006; received in revised form 26 September 2006; accepted 6 April 2007

Abstract

This study examined the carbon budget of a *Eucalyptus delegatensis* forest over four years under contrasting weather conditions by using a comprehensive forest-growth model (CenW 3.1). Model parameterisation was constrained through multiple measurements, including daytime eddy flux measurements of CO_2 and water vapour exchange, estimates of above- and below-ground biomass pools, growth rates measured through stem-diameter increments and measurement of specific ecosystem processes, such as litter fall and soil respiration rates.

The resultant estimates of net ecosystem exchange ranged from an uptake of 4.0 t C ha^{-1} $year^{-1}$ in a year with adequate rainfall to a loss of 0.4 t C ha^{-1} $year^{-1}$ in a year affected by drought and insect damage. The simulations indicated that this reduction in carbon gain was primarily due to insect damage rather than a direct consequence of water shortage. Under good growing conditions, carbon gain accumulated equally in stem wood and other biomass pools while soil organic carbon and woody litter were gradually decreasing following harvesting that had occurred 20 years earlier. Under more stressful conditions, net biomass increments decreased, while soil organic carbon and woody litter increased because of greater litter inputs and because drier conditions inhibited decomposition.

Modelled estimates of photosynthesis and net ecosystem exchange were similar to estimates from eddy flux observations alone provided that it used a novel routine for deriving night-time carbon fluxes. Estimates of net ecosystem exchange derived in the present work were, however, substantially lower than previous estimates that had been derived using a more traditional analysis of eddy flux data.

This study showed that detailed physiological modelling is a valuable technique for combining all available site information as well as further constraints based on broader scientific principles and considerations of the conservation of mass. It can thus provide a powerful constraint on the overall site carbon budget of an ecosystem.
© 2007 Elsevier B.V. All rights reserved.

Keywords: Carbon exchange; CenW; Eddy covariance; Insect damage; Model; Net ecosystem exchange; Photosynthesis; Soil respiration

1. Introduction

With a global concern over increasing CO_2 concentrations in the atmosphere, there is strong interest in understanding the factors that determine

* Corresponding author. Present address: Landcare Research, Private Bag 11052, Palmerston North, New Zealand.
Tel.: +64 6 353 4902; fax: +64 6 353 4801.
E-mail address: KirschbaumM@LandcareResearch.co.nz (M.U.F. Kirschbaum).

0168-1923/$ – see front matter © 2007 Elsevier B.V. All rights reserved.
doi:10.1016/j.agrformet.2007.04.002

carbon fluxes between the atmosphere and the biosphere. A global network of over 400 eddy covariance flux towers (FLUXNET) has now been established to continuously monitor the exchange of CO_2, water vapour and energy in a range of ecosystems (http://www.fluxnet.ornl.gov/fluxnet). These measurements provide a wealth of data, with particular value being the continuity of measurements across seasons under varying weather conditions, and the ability to integrate fluxes across whole stands (e.g. Baldocchi and Wilson, 2001; Baldocchi, 2003; Wang et al., 2004; Medlyn et al., 2005). By applying this technique to stands with very different properties and subject to different weather patterns, it is hoped to gain new insights into the main factors that control the carbon exchange of plant canopies.

If good on-site understanding of carbon fluxes can be combined with remotely sensed information, it allows the construction of a global mosaic of gas exchange fluxes and estimation of global totals (Running et al., 1999; Turner et al., 2005). This approach holds the promise to better understand the role of the biosphere in the global carbon cycle.

However, like all sophisticated measurement techniques, eddy covariance faces several technical and methodological challenges (Finnigan et al., 2003), especially for the estimation of night-time fluxes (Aubinet et al., 2003, 2005; van Gorsel et al., 2007). When there are no other methods to directly and independently calibrate the fluxes calculated by eddy covariance, it is therefore problematic to solely rely on this single technique for the estimation of annual gas exchange fluxes.

To build greater confidence in estimates of carbon exchange, some projects have combined eddy flux measurements with a range of other measurements related to site carbon budgets in order to more tightly constrain annual carbon budgets (e.g. Curtis et al., 2002; Schelhaas et al., 2004). There is a challenge, however, in combining diverse observations to constrain site budgets, and more or less sophisticated models have been used for such purposes (Hanson et al., 2004).

In the present work, we combined a range of ecosystem measurements, including eddy flux measurements, in-situ observations of dynamic stand properties, such as tree growth, foliage dynamics and soil and plant respiration rates and measurements of the sizes of various biomass, litter and soil organic matter pools. All these observations were compared with corresponding values simulated by the full ecosystem model CenW. Hence, each measurement provided constraints not only through their observed temporal patterns, their dependence on environmental driving variables such as temperature or moisture status, but, most importantly, also through their absolute magnitudes. Combining all these measurements thereby provided tight constraints on the estimate of the system's total carbon budget and helped to understand the drivers of the ecosystem's carbon exchange.

2. Measurements and climate

The study site, referred to as "Tumbarumba", is located within the Bago State Forest in south-eastern New South Wales, Australia (35°29′S and 148°9′E) at an elevation of 1200 m. This native forest has been the subject of extensive previous studies on various aspects of forest productivity and its controlling factors. The forest receives about 1500 mm annual rainfall, but with considerable inter- and intra-annual variation (Leuning et al., 2005), and experiences an average mean temperature of about 8.0 °C.

Most of the forest had naturally regenerated after logging in about 1940, and is currently a moderately open, wet sclerophyll forest, about 40 m tall, in which the dominant species are *Eucalyptus delegatensis* (R.T. Baker) and *Eucalyptus dalrympleana* (Maiden). There is also a small number of trees that are older than 60 years and an understorey with a patchy cover of shrubs and a full cover of grasses. Forest cover and species composition are similar in all directions for more than 5 km around the eddy flux tower. The soil is classified as an acidic, eutrophic, red dermosol, 3–4 m deep which includes a weathered C horizon, and has moderate nutrient status and amounts of stored carbon (McKenzie and Ryan, 1999).

Micrometeorological measurements of the fluxes of CO_2, water vapour and heat were made at a height of 70 m on a single tower. Ancillary measurements included temperature, humidity, solar radiation, wind speed and direction, rainfall and soil temperature. Full details of instrumentation and results were presented by Leuning et al. (2005). Temperature measurements at 1 m height were available from September 2001 to December 2004 and were used for the simulations. For periods when data from 1 m height were not available from the tower site, we used data from a nearby weather station at Laurel Hill which is located 8 km from the tower site at an elevation of about 1000 m. Appropriate corrections were used for these data derived from periods with overlapping data.

For the period from 1940 to 2000, rainfall records for the tower site were reconstructed from rainfall measured at the Tumbarumba Post Office, located

about 40 km south of the flux tower, and at an elevation of 750 m. Long-term temperature records were obtained from Canberra, about 130 km to the north-east of the tower site and at an elevation of 500 m. Temperatures and rainfall were corrected for the systematic differences between these locations, and periods with overlapping records indicated that the data could be used with reasonable confidence.

Solar radiation was measured at the flux tower from February 2001 to December 2004. Those data were used to fit a model based on latitude, day of the year, minimum and maximum temperatures and rainfall as described in Appendix A. That fitted model was then used to generate solar radiation for 1940–2000, and for brief periods during the experimental period when data were missing.

We used detailed eddy covariance measurements that have been maintained since March 2001 (Leuning et al., 2005) and ground-based measurements that have been reported by Keith and Wong (2006) and Keith et al. (2005). Carbon pools and fluxes were measured in 30 plots in the source area surrounding the tower. Above- and below-ground biomass was estimated from inventories of tree diameters measured in all plots and allometric relationships derived from destructive sampling of a number of harvested trees.

The pool of forest floor litter layer was measured in quadrats randomly located in each plot with all material weighed and carbon concentrations determined. Coarse woody litter was estimated from measurements of volume and density of samples encountered along linear transects in each plot. Soil cores were taken to 2 m depth, with carbon concentration and bulk density measured in depth increments and then summed to obtain totals for the soil. Litter fall was collected monthly in each plot and separated by hand into leaf and other litter. Leaf area index was estimated using hemispherical photographs and independently from allometric relationships based on stem diameters. Annual tree growth was determined from diameter increments of all trees in the plots, and converted to biomass using the allometric equations referred to above.

Soil respiration over 24 h was measured in chambers in each of the 30 sample plots with the soda-lime static absorption technique which was thoroughly tested before use (Keith and Wong, 2006). Plant respiration was measured by leaf, root and stem chambers during three campaigns in September and November 2003 and February 2004. Stem-respiration measurements were taken at the ambient temperature at the time and with temperature varied over a range of about 10–15 °C on each occasion. Short-term temperature responses and temperature acclimation was estimated from these data.

Intensive measurements at the study site were taken between February 2001 and December 2004. The weather in those years ranged from a year with above-average rainfall (2001) to a severe drought which occurred over all of eastern Australia in the period March 2002–May 2003.

3. Modelling

The simulations used the model CenW 3.1 as described by Kirschbaum (1999, 2004) and Kirschbaum and Paul (2002). The model had originally been developed and parameterised for *Pinus radiata*, but its generic structure has allowed its ready application for a range of plant types and environments (Kirschbaum et al., 2003; Kirschbaum, 2004). The model and its source code are available at: http://www.kirschbaum.id.au/Welcome_Page.htm, with a full list of relevant equations available at: http://www.kirschbaum.id.au/CenW_equations.pdf.

The model runs on a daily time step and simulates stand characteristics, such as leaf-area development, stand height, basal area development, litter fall and exchange of both water and CO_2. The model recognises no sub-division into under- and overstorey, but simulates the whole stand as a single unit. Stand-level dynamics are explicitly linked to carbon and nitrogen cycling in the soil and plants. This linkage allows multiple measurements to constrain estimates of growth and carbon exchange of the stand at daily or longer time scales.

The model can be easily run over periods of many decades, which was necessary for the stand at the Tumbarumba forest, of which the dominant trees were estimated to be about 60 years old. As external drivers, the model requires daily minimum and maximum temperature, solar radiation and precipitation. The model is initialised by setting the size of plant and soil organic matter pools to values with which measured site observations are best reproduced for the given environmental drivers. The model then provides a large number of outputs that can be compared against the corresponding field observations.

A number of modelling changes were required and are described below. Other new routines required for the present simulations are described in Appendix B. A set of key parameter values is given in Appendix C. A brief description of the model is given in the following, but readers are referred to the original publications or the web site for full modelling details.

3.1. Photosynthesis and respiration

Photosynthetic calculations were based on combining the photosynthesis model of Farquhar and von Caemmerer (1982) with the simple stomatal model of Ball et al. (1987). Maximum photosynthetic capacity was controlled by foliar nitrogen status and further restricted by temperature limitations, water stress and damage from pests and diseases as discussed below.

These instantaneous leaf-level equations were then scaled up to the canopy and to a daily time scale using the equations of Sands (1995). These equations calculate daily canopy photosynthesis from parameters of single-leaf photosynthetic light response, canopy extinction coefficient, leaf area index, day length and daily solar irradiance. The calculations assume that light absorption within the canopy follows Beer's law, that maximum photosynthetic rate within the canopy is proportional to light absorption and that light varies sinusoidally throughout the day. It is an efficient algorithm for calculating canopy photosynthesis while minimising systematic scaling errors.

Plant (autotrophic) respiration was modelled with a short-term temperature dependence modified through acclimation (Gifford, 1995; Atkin et al., 2005) that could negate the short-term temperature response. The functional form of that relationship has been described by Kirschbaum (2005) and was further refined for the present work (Appendix B).

3.2. Phenology routine

While eucalypts are evergreen, the pattern of foliage production and loss nonetheless follows a distinct seasonal pattern, with both leaf fall and new foliage production occurring mainly over the summer months. The time of peak litter fall varied between years, with peak litter fall occurring earlier in a warmer year. This pattern of litter fall could be well described as a function of heat sums of mean daily temperatures above 10 °C.

New growth was calculated by accumulating new carbon in a pool of leaf primordia throughout the year over periods when conditions were conducive to new growth. These primordia were then converted into new leaves at times that corresponded to the observations of the occurrence of new leaves. This was also physiologically linked to the calculation of heat-sums.

3.3. Insect damage

It was apparent that trees at the study site could at times be subject to extensive insect damage. This included a period of severe attack by phasmatids (stick insects; *Didymuria violescens* Leach) over the period from 1955 to 1964, with estimated growth reductions of up to 50%, and tree death of up to 50% in some years (State Forest of NSW, unpublished). These episodes of insect damage were included in the simulations over the early period of stand development.

During the experimental period, trees were subject to attack by psyllids (*Cardiaspina* spp.). These insects suck leaf sap and cause necrosis. They also form protective covers over their bodies that prevent sunlight from reaching the leaf. Under severe circumstances, that damage can induce leaf fall. Damage to leaves occurs in a sequence of forms, usually beginning with sap-sucking and removing assimilate over the summer months and covering patches of the laminae with white, lacey lerps. In severe cases, this progresses to necrosis of leaf tissue leaving pinkish-brown patches and inducing abscission in autumn (Farrow, 1996).

In the context of understanding a site's carbon budget, sap sucking causes a diversion of photosynthate from trees to insects from where the majority is lost by respiration. Leaf necrosis and associated psyllid coatings also reduce photosynthetic carbon gain. Enhanced leaf fall reduces leaf area which further reduces photosynthetic carbon gain. Increased litter input rates also result in subsequently increased heterotrophic respiration. Each of these effects was independently simulated in the model as described in Appendix B, with the timing and parameters given in Table C2 of Appendix C.

3.4. Water relations

Transpirational water loss was calculated with the Penman-Monteith equation with canopy conductance explicitly linked to photosynthetic carbon gain based on the Ball–Berry model (Ball et al., 1987). Preliminary work indicated that it was important to correctly simulate water relations of the litter and of different layers in the mineral soil. This was important for simulating both evapotranspiration and litter and soil respiration rates that responded strongly to the gradual drying of the soil and litter layers over the days since the last rain event. Details of the new calculation routines are given in Appendix B.

Organic matter dynamics were also simulated separately for the litter and each soil layer, with the same calculations for each organic matter pool done independently for each layer. This included a separate assessment of the extent of moisture limitation for decomposer activity in each layer.

3.5. Allocation

Plant stands were sub-divided into foliage, branches, sap- and heartwood, bark, pollen and fruiting bodies, fine and coarse roots, soluble carbohydrate and leaf primordia. This sub-division was found necessary as each of these pools is unique with respect to their nutrient concentration, longevity, physical location (above- or below-ground) and physiological function.

Carbon allocation to different plant organs was determined by plant nutrient status, tree height and species-specific allocation factors. It was assumed that the ratio of above to below-ground allocation increased with foliar nitrogen concentration and that the allocation ratio of stem wood to foliage increases with increasing tree height, but that allocation ratios between branches, bark and coarse roots and stem wood remained invariant with height or nutrient status. Nitrogen allocation was treated in a similar way except that it was further assumed that the nitrogen concentration in each biomass component scaled linearly with foliar nitrogen concentration with different proportionality terms for each component.

3.6. Organic matter dynamics

Organic matter dynamics were calculated with a version of the CENTURY model (Parton et al., 1987) that had been slightly modified to better describe the dynamics of forest soils and litters with their often wider C:N ratios than found in agricultural and grassland soils (Kirschbaum and Paul, 2002). As such, the model contains a complete and coupled nitrogen cycle, with nitrogen taken up by stands following decomposition and nitrogen mineralisation. Nitrogen was then either retained in plant pools or returned to the soil in senescence of plant organs, especially from foliage and fine roots.

3.7. Model fitting

The present work aimed to get the best constrained estimates of net ecosystem carbon exchange (NEE) over four successive seasons. Parameter values of the model were constrained to remain within plausible bounds and thus provided one constraint on possible net ecosystem exchange rates. Where possible, parameters were prescribed by independent measurements. Where independent parameter estimates were not available, parameters were varied to get best agreement with all available observations. The relevant output of this work was thus the estimation of NEE, whereas parameter values were primarily a tool used to constrain NEE, but not themselves reliably estimated outcomes of this work.

3.8. Statistical analysis

The goodness of fit in respective comparisons between model and data was assessed by calculating model efficiency, which is the extent of variation explained by the model (or by a 1:1 line). Hence, it assesses not only the closeness of the correlation between model and data, but also whether there is any consistent bias in the relationship. High model efficiency can only be achieved when model and data are consistently closely related and when there is little systematic bias in the model.

Formally, model efficiency, EF, was calculated as (Nash and Sutcliffe, 1970; Soares et al., 1995):

$$\mathrm{EF} = 1 - \frac{\sum (y_\mathrm{o} - y_\mathrm{m})^2}{\sum (y_\mathrm{o} - \bar{y})^2} \quad (1)$$

where y_o are the individual observations, y_m the corresponding modelled values and $\bar{y}$ the mean of all observations.

The model was run from 1940 through to the end of the experimental period in December 2004, and model efficiencies were calculated simultaneously for each available observation. Parameters were then optimised to maximise the average of model efficiencies of all observations.

4. Results and discussion

4.1. Initial pool sizes

The past history of the experimental forest is incompletely known and recorded, but it is most likely that most of the trees of the current stand were established in about 1940. Dendrochronological observations indicate that some trees were up to 90 years old but the contribution of this small number of older trees was ignored for the present simulations. More detailed records exist for harvesting and insect damage from 1950 onwards.

The model was able to adequately describe the size of the stand at the beginning of the experimental period, with the size of all biomass pools agreeing with measurements (Fig. 1). The simulated growth up to that point clearly shows the period of extensive insect-induced mortality in the late 1950s to early 1960s and a period of harvesting in the 1980s. Modelled stem-wood

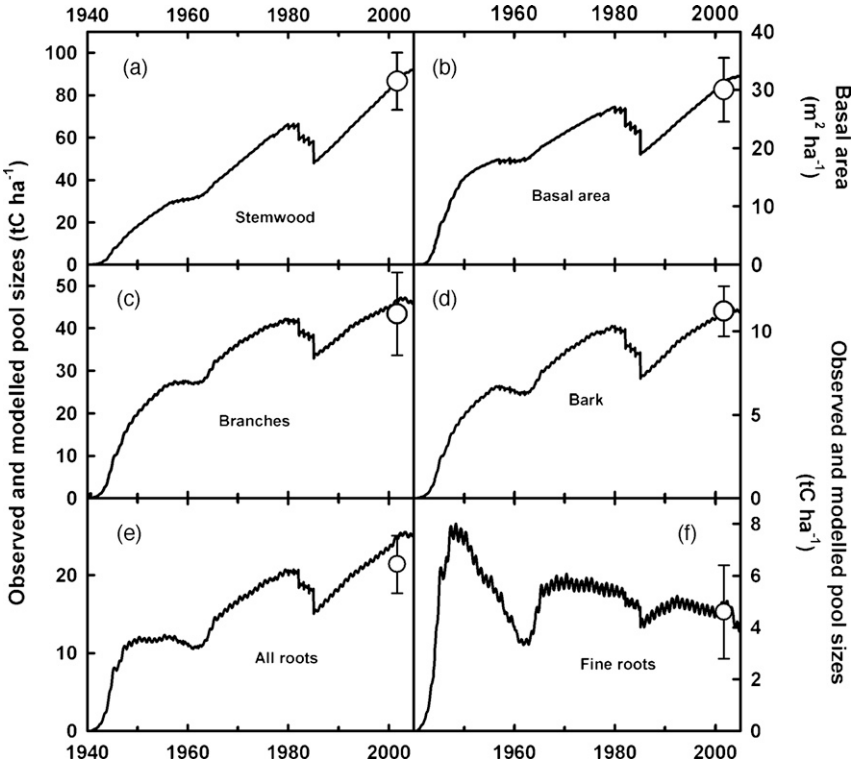

Fig. 1. Observed and modelled stemwood (a), basal area (b), branch (c), bark (d), total-root (e) and fine-root biomass (f). Lines show modelled data and the symbols give the observed pool sizes measured at the beginning of the experimental period. Error bars give upper and lower 95% confidence limits.

and coarse-root pools were still increasing after 60 years of growth whereas branches and bark were close to their maxima, with new growth matched by loss and turn-over of existing biomass. Fine roots reached their peak mass during early stand development and their mass has been decreasing slightly over the latter stages of stand growth. These patterns were largely caused by the different turn-over times of different biomass components, with stem wood being lost only during tree death, whereas there was continuous turn-over of the other biomass pools.

The simulations from 1940 to 2000 also provided a history of litter production, especially coarse woody-litter production, and organic matter dynamics that provided initial sizes and dynamics of these quantitatively important pools (Fig. 2). Running the model for an extended period leading up to the experimental period ensured that the resultant pool sizes and their changes were modelled in an internally consistent manner.

These various pools of soil organic carbon and surface litter could be adequately modelled to agree with the measurements at the start of the experimental period. As the model contains a fully coupled nitrogen cycle, these soil organic carbon dynamics also constrained the nitrogen supply to trees.

Changes in the size of these pools, especially coarse woody litter, also constituted an important component of the carbon balance of this forest system. It was assumed that the site had received a large amount of coarse woody debris from killed trees when the majority of the stand was established in 1940. Decay of that debris led to reductions in woody and other litter pools over the following 10–20 years. Soil carbon also decreased over that period because litter input rates were low during early stand development. Litter and soil carbon amounts decreased over the late 1950s to early 1960s in response to a severe episode of insect-induced mortality that also reduced litter production for a number of years.

During the 1980s, the stand was heavily thinned (see Fig. 1) which led to a large input of logging debris. This pool was slowly diminishing over the experimental period as a result of slow on-going decay with little further inputs. Soil carbon amounts also changed slightly in response to changing litter input rates.

Over the first 60 of simulation, individual-tree mortality was calculated based on application of the

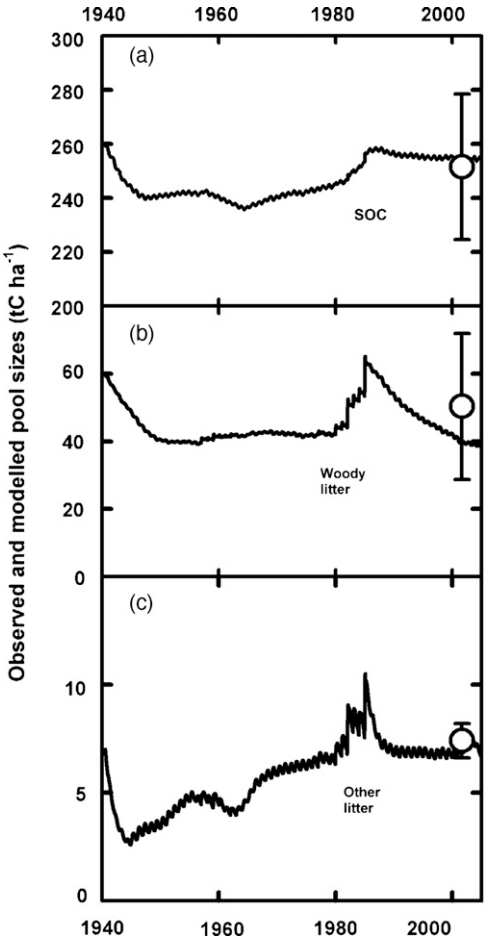

Fig. 2. Observed and modelled pools of soil organic carbon (a), above-ground woody litter (b) and other surface litter (c). Lines show modelled data and the symbols give observed pool sizes at the start of the experimental period. Error bars give upper and lower 95% confidence limits.

three halves self-thinning law (Oliver and Larson, 1990; Pretzsch, 2002). Observations in a range of forests in the vicinity of the experimental site confirmed that that relationship gave an excellent description of the self-thinning characteristics of these forests (Fig. 3).

The stocking and average size of individual trees in all measured plots in these forests could be described very well by a linear relationship on a log-log plot with a slope close to −1.5 as predicted by the self-thinning law. The experimental site itself fell slightly below the fitted line, which may reflect true site differences in carrying capacity or simply constitute random variation.

The simulations yielded results for stand stocking and average mass of individual trees that were very close to the data measured at the experimental site. This provided important constraints in terms of stand growth dynamics, carbon losses due to mortality, coarse-litter

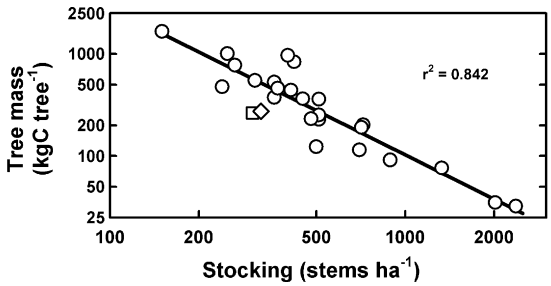

Fig. 3. Relationship between individual-tree mass and stand stocking. Data are for 24 additional forest plots in the same region. The experimental site is designated as the square symbol and the modelled data as the diamond, which fall on almost the same point. The fitted line is described as: $T = \exp[14.57 - 1.44 \ln(n)]$, with '$T$' the mass of individual trees and 'n' the number of stems per hectare.

production, and it ensured an internally consistent development of tree sizes and stand stocking.

4.2. Dynamic observations

During the experimental period, a range of processes were measured in detail. The first of these was leaf-litter fall (Fig. 4). Its rates generally peaked in mid-summer, with leaf-litter fall rates at that time of the year being an order of magnitude greater than over the winter months. Production of new foliage normally coincided with the shedding of old foliage so that leaf area index remained fairly constant over that period (data not shown).

In 2003, there was a secondary peak of high leaf loss in autumn (April–May). Visual inspection of leaves indicated that this was associated with leaf damage by psyllids. The model, with inclusion of heat-sum based annual cycle of leaf loss and the specific insect-induced increased leaf shedding in the summer of 2003, was able to account for 94.5% of observed variation. The pattern

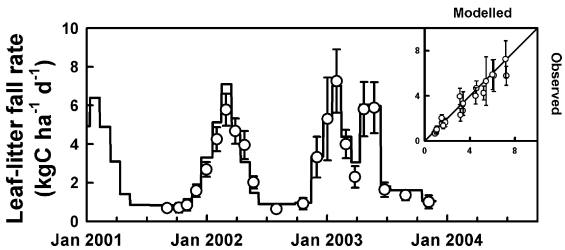

Fig. 4. Observed and modelled time course of leaf-litter fall. The insert gives observed vs. modelled data with a 1:1 line. Error bars give upper and lower 95% confidence limits. The secondary peak in litter fall in 2003 was due to insect (psyllids)-induced leaf mortality. Modelled data were averaged over the same integration periods over which experimental data had been collected. Model efficiency (EF) was 0.945, and the observed (O) vs. modelled (M) was best described by O = 0.939M + 0.03 (r^2 = 0.955).

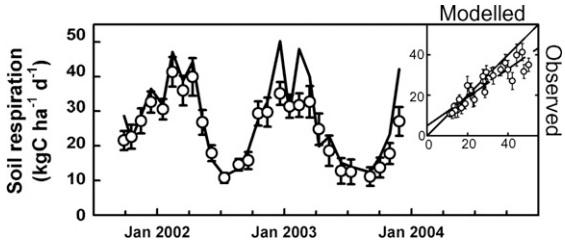

Fig. 5. Time course of observed and modelled soil (incl. litter) respiration. The insert shows observed vs. modelled data, with the solid line a 1:1 line and the dashed line a line of best fit. Error bars give upper and lower 95% confidence limits. EF = 0.721; O = 0.70M + 4.96 (r^2 = 0.830).

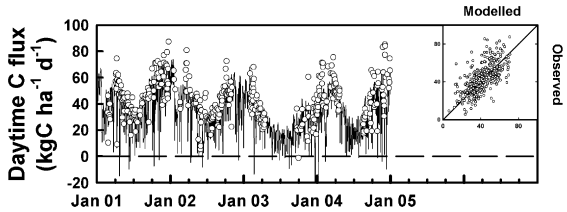

Fig. 6. Observed and modelled daytime net carbon exchange rates. The insert shows observed vs. modelled data, with the line being a 1:1 line. Observed data were obtained with eddy-flux methods. Observed average net carbon uptake was 43.4 kg C ha^{-1} day^{-1} and the average of simulated values for the same days was 41.2 kg C ha^{-1} day^{-1}. EF = 0.410; O = 0.793M + 10.8 (r^2 = 0.464).

of leaf-litter production provided important constraints on photosynthesis and carbon allocation to foliage development, nutrient cycling and soil respiration rates.

Soil respiration (including both heterotrophic and root respiration) was also well described in both its absolute magnitude and its seasonal pattern (Fig. 5). There was, however, a tendency for the highest summer rates to be overestimated by the model. The temperature-limited rates over autumn, winter and spring appeared to be modelled well, but there were difficulties in fully capturing the dependence on soil moisture that largely controlled rates in summer.

While the seasonal pattern was largely dominated by temperature and soil moisture, seasonally varying litter input (as shown in Fig. 4) and root respiration also added to temporal variability. The soil was generally wet over the winter months so that moisture generally constituted no limitation to heterotrophic respiration over that time. During the summer months, however, when temperatures were favourable, the soil was often too dry for high rates of heterotrophic respiration. Hence, the pattern of soil respiration was strongly determined by the timing of rainfall events and the rate at which the soil subsequently dried out (Tang et al., 2005).

In describing this seasonal pattern, the model used a temperature response function for heterotrophic respiration obtained from an earlier literature survey (Kirschbaum, 2000). Moisture relations were largely based on the work of Keith et al. (1997) that had been conducted in a similar forest type, but were further tuned to best describe the patterns observed in the present work.

One of the most important comparisons for the present work was that between the model and data observed from eddy flux measurements (Fig. 6). Flux tower observations were collected continuously and integrated into hourly fluxes. For the comparison shown here, these hourly data were summed over the daylight hours to give estimates of summed total daily fluxes. Data were used only for days when complete data were available for every hour of daylight. This provided a large number of individual data points for comparison, and enough data to follow seasonal trends over several years. There were, however, also many gaps over random periods due to equipment failure or systematically during rainy periods (see below).

Comparisons were fairly good, with the model giving a similar average carbon uptake rate as that observed. It also replicated the seasonal and day to day changes in net carbon flux (Fig. 6). Overall, model efficiency was 0.410, with a slight bias for the model to underestimate the lowest and overestimate the highest net fluxes.

The simulations suggested that on some days, carbon was lost even during the day, but this was observed on only one occasion. Fig. 6 also gives the apparent impression that the model might systematically underestimate observed fluxes. However, a more detailed examination of the data showed that negative net carbon exchange rates were mainly modelled on days when observations were missing, and that there is, in fact, no systematic difference between model and data on days when measurements had been obtained (Fig. 7).

There is a systematic problem in that data from the turbulent sensors (i.e. sonic anemometers and open-path CO_2 analysers) are compromised during precipitation events. Yet, rainy days tend to be days when

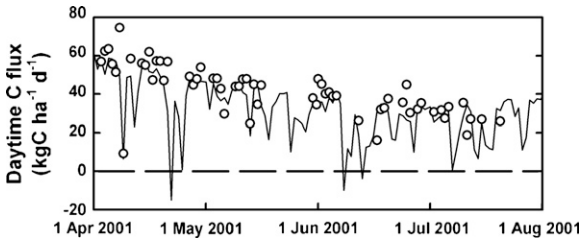

Fig. 7. Expanded scale of observed and modelled daytime carbon exchange for a four-month period in 2001. Over the whole measurement period, modelled average daytime net carbon uptake was 33.1 kg C ha^{-1} day^{-1}, but 41.2 kg C ha^{-1} day^{-1} if only those days were considered for which measurements were available.

photosynthetic carbon gain is low because of cloudy conditions, and soil respiration is high because the soil and litter layer are freshly wetted. Hence, there were no observations on many days with negative modelled values, such as on 22 April, 8 June and 13 June (Fig. 7).

Over the whole experimental period, average modelled net C uptakes rates were 20% higher for days with climatic conditions for which observations were available than for the average of all days. It raises the potentially very important concern that eddy flux data might systematically overestimate net carbon uptake rates by excluding observations under climatic conditions that lead to low net uptake rates.

Fig. 8 compares the net ecosystem exchange determined with the multiple constraints approach described above with estimates calculated from the flux measurements on the site that had been analysed with the revised data processing approach developed by van Gorsel et al. (2007). While the two estimates are based on quite different approaches and assumptions, they are not fully independent as both approaches used the same daytime eddy flux measurements for their respective photosynthesis and NEE estimates.

For night-time carbon losses, the present work relied on algorithms constrained by direct measurements of soil and plant respiration to infer and sum annual totals, whereas van Gorsel et al. (2007) used an innovative approach to calculate night-time carbon losses from

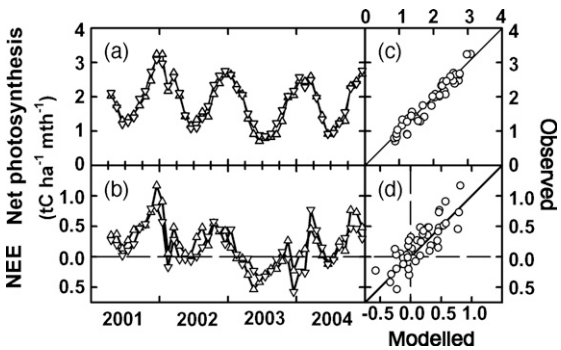

Fig. 8. Comparison of estimates of monthly photosynthesis (a) and net ecosystem exchange (NEE) (b) estimates using either just flux tower observations (Δ) or the full model simulation (▽) as described here, and observed vs. modelled data (c, d). Revised flux-tower estimates were obtained with the method described by van Gorsel et al. (2007). Cumulative totals over the 45 months for net photosynthesis were 84.6 t C ha^{-1} (flux tower) and 82.6 t C ha^{-1} (CenW), respectively, and 9.7 t C ha^{-1} (flux tower) and 6.9 t C ha^{-1} (CenW) for net ecosystem exchange. Symbols in (a) and (b) have been linked by lines for better visualisation of trends. Lines in (c) and (d) are 1:1 lines. Model efficiencies are 0.937 and 0.647 for photosynthesis and NEE comparisons, respectively, and lines of best fit are given by $O_p = 1.007M_p - 0.05$ ($r^2 = 0.941$) for photosynthesis, and by $O_n = 0.91M_n + 0.08$ ($r^2 = 0.687$) for NEE.

eddy flux measurements that were confounded by the effects of horizontal and vertical advection.

The approach, described in detail in van Gorsel et al. (2007), is based on the hypothesis that turbulent exchange, storage of CO_2 in the canopy and advection act at different time scales. The total exchange of CO_2 between the forest and the atmosphere is dominated by the turbulent exchange during periods of high atmospheric turbulence. At other times, such as on calm nights when stable atmospheric conditions inhibit mixing, respired CO_2 can build up in the airspace of the forest canopy. If the site is located on even gently sloping terrain, as our experimental site is, then density-driven flows entrain this CO_2 and transport it down slope so that it is not measured by the turbulence sensors atop the instrument mast.

Experimental data showed that the different components of the fate of respired CO_2 (in-canopy storage, and turbulent and advective fluxes) operated on different timescales so that there is a period in the early evening after photosynthetic uptake has ceased when advection is negligible and the turbulent plus storage terms provide the most reliable measure of nocturnal carbon efflux. Detailed comparisons with independent respiration measurements from chambers confirmed the validity of that approach.

The complete data set of the maximum hourly observed nocturnal respired fluxes was then used by van Gorsel et al. (2007) to parameterise an algorithm for estimating respired night-time carbon efflux. These derived nocturnal fluxes were then combined with measured daytime turbulent plus storage fluxes to determine daily, monthly and annual estimates of photosynthetic carbon gain and net ecosystem exchange. Gaps in the flux time series were filled using a Michaelis-Menten type parameterisation to develop non-linear relationships for CO_2 exchange as a function of shortwave radiation.

Agreement between the two methods was excellent for estimating net photosynthesis in both the magnitude of the response, the seasonal pattern and the slight reduction in rates during the period of drought and insect damage in 2003 (Fig. 8a and c).

Agreement between the methods was also good for net ecosystem exchange (Fig. 8b and d), again largely agreeing in the overall magnitude and showing the same periods of high and low or even negative values in some months or extended periods. The correlation between estimates for the two methods is weaker for NEE than for net photosynthesis, which indicates that the more variable factors are likely to lie in carbon losses from either autotrophic or heterotrophic

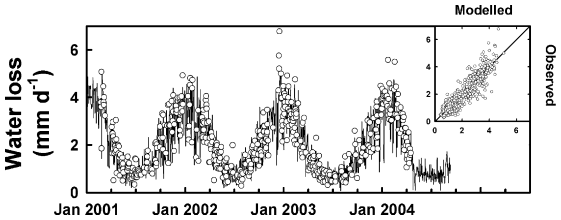

Fig. 9. Observed and modelled daily evapotranspiration rates. The insert shows observed vs. modelled data, with the line being a 1:1 line. Evapotranspiration includes tree transpiration, soil and litter evaporation and canopy evaporation of intercepted rainfall. Observed data were only used for days when complete records were available. EF = 0.802; O = 0.985M − 0.06 (r^2 = 0.824).

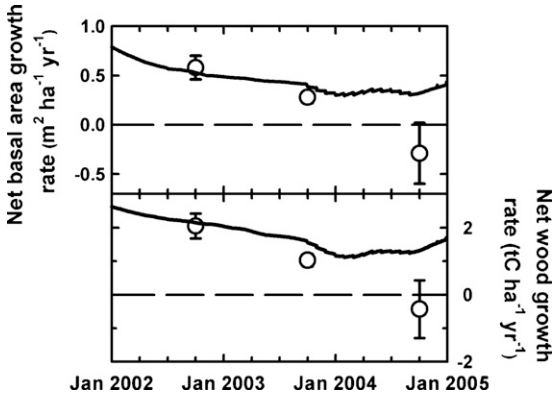

Fig. 10. Observed and modelled net basal area and net wood growth rates. Data include new growth minus losses due to mortality. All observations and model results correspond to growth over the preceding 12 months from respective dates in the figure. Error bars give 95% confidence limits.

respiration rather than for the processes of carbon gain.

Cumulative NEE was also higher for tower-derived estimates (9.7 t C ha^{-1} over 45 months) than for CenW-derived estimates (6.9 t C ha^{-1}). These differences may well be due to the missing observations from the eddy flux method on wet days (see Fig. 7).

Eddy flux measurements were also used to calculate evapotranspiration fluxes, and comparison against model output gave very high agreement in average magnitude as well as seasonal patterns and day to day variations, with a model efficiency of 0.802 (Fig. 9). This included separate modelling of the three contributing fluxes: transpiration, soil and litter evaporation and direct evaporation of water intercepted by the canopy.

Reliable modelling of water fluxes is important for calculating both carbon and water budgets. Daily water fluxes determine the overall water budget of the stand and thereby determine the timing and severity of water stress. Water dynamics also affect the period over which the litter and upper soil layers are wet and can allow high decomposer activity with resultant respiratory carbon losses.

The model was also able to simulate net wood growth over the experimental period (Fig. 10). Net wood growth was reduced over 2003 and the early part of 2004 due to reduced carbon gain and increased losses due to mortality, which were prescribed in the model based on observed mortality. Model simulations that are shown in detail below indicate that these changes were largely caused by insect damage.

While the magnitude of net wood increment was modelled adequately, the model suggested a faster recovery than observed after conditions improved during 2004. Net carbon gain had increased to higher values again (Fig. 8), and the model allocated a similar proportion of that extra carbon to new wood growth, which was more than observed. This may indicate that the physiological processes were inadequately captured by the model. Hence, stands may have preferentially allocated carbon to fine roots and foliage and less to stem-wood production in this recovery period whereas the model assumed allocation proportions to have remained the same throughout.

4.3. Summary of fluxes

After having shown that the different components of the system's carbon exchange compared well with their corresponding measurements, it was then possible to use the model to express individual physiological components on a daily basis during the experimental period (Fig. 11).

Photosynthetic carbon gain followed a strong seasonal cycle (Fig. 11a), with maximum uptake rates in summer when temperatures were favourable and solar radiation was high. Winter rates were sizeable even when daytime temperatures were close to 0 °C. The site is relatively wet by Australian standards and the model indicated that there was no water stress over the summer months in 2000–2001 and 2001–2002. In the summers of 2002–2003 and 2003–2004, however, insect damage compounded by the effect of drought lowered photosynthetic rates below those in the previous two years.

Autotrophic respiration followed a seasonal cycle that paralleled, but was of lesser amplitude than the seasonal cycle of carbon gain (Fig. 11b). Detailed physiological work has often suggested that temperature acclimation can be completed within days (Gifford, 1995; Atkin et al., 2005), but the measurements in the current experiment suggested only relatively slow

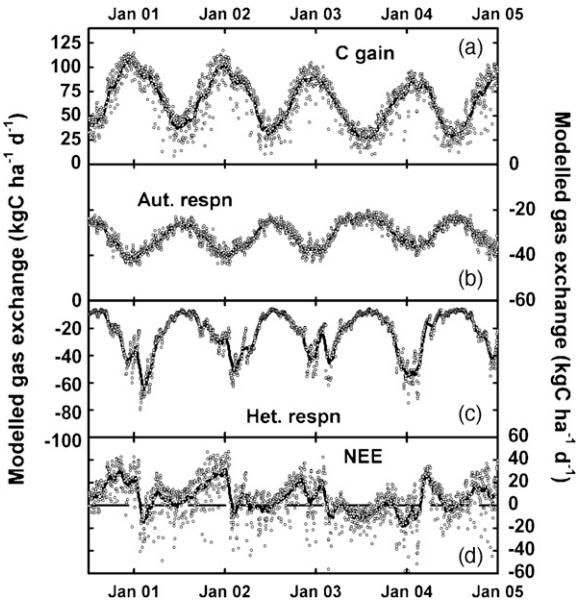

Fig. 11. Photosynthetic carbon gain (a), autotrophic respiration (b), heterotrophic respiration (c), and net ecosystem exchange (d) modelled over the experimental period. Symbols show daily values and lines show 31-day running means. Positive values designate carbon uptake.

temperature acclimation over a period of slightly over a month. This was constrained by comparison with eddy flux data (Fig. 6) and short-term chamber-based measurements during three measurement campaigns (data not shown).

Heterotrophic respiration also followed a strong seasonal pattern (Fig. 11c), with rates being very low in winter because of the strong temperature dependence of heterotrophic respiration (Kirschbaum, 2000). Summer rates increased strongly with increasing temperature as long as the soil remained wet, but were depressed by drying of the litter and upper soil layers (Keith et al., 1997; Tang et al., 2005). Hence, activity was quite high in the summers of 2000/2001 but markedly lower in the dry summers of 2001/2002 and 2002/2003 before increasing again in 2003/2004.

Heterotrophic respiration was much more sensitive to limitations by soil moisture than photosynthetic carbon gain because plant water relationships were buffered through an extensive root systems that allowed plants to use water from the whole soil profile whereas decomposer activity was concentrated in the surface litter and upper-most soil layers and could only continue at high rates when those layers were moist enough. Consistent, with that, heterotrophic respiration over the summer months often showed strong short-term responses to wetting and drying cycles (see also Tang et al., 2005).

Net ecosystem carbon exchange consequently followed quite an irregular pattern, with extended periods of net carbon gain followed by periods with more neutral balance and even carbon losses (Fig. 11d). While average NEE was positive over most periods, values fluctuated around 0 between January 2003 and January 2004. Individual days often deviated strongly from longer-term means. In particular on some wet and cloudy days, NEE was sometimes substantially less than monthly means because photosynthetic carbon gain was reduced by low radiation but heterotrophic respiration was stimulated by wetting of the litter and upper soil layers.

4.4. Net ecosystem exchange

Cumulative net ecosystem exchange often increased until about the middle of summer and then stopped abruptly and remained flat for autumn and early winter (Fig. 12). This was caused partly by the influx of fresh foliage litter that provided the labile substrate for an accelerated rate of heterotrophic respiration but it was primarily due to the occurrence of rainfall that wetted the top of the soil and provided suitable environmental conditions for high respiratory activity in the soil.

Summing the net ecosystem exchange rates over full years (starting from 1 July) showed that the system was a strong carbon sink in 2000/2001 and 2001/2002, with gains of 4.0 and 3.5 t C ha^{-1} $year^{-1}$, respectively (Fig. 12). The system had a smaller gain of 1.5 t C ha^{-1} $year^{-1}$ in 2002/2003 and was a source in 2003/2004 when it lost about 0.4 t C ha^{-1} $year^{-1}$. There was

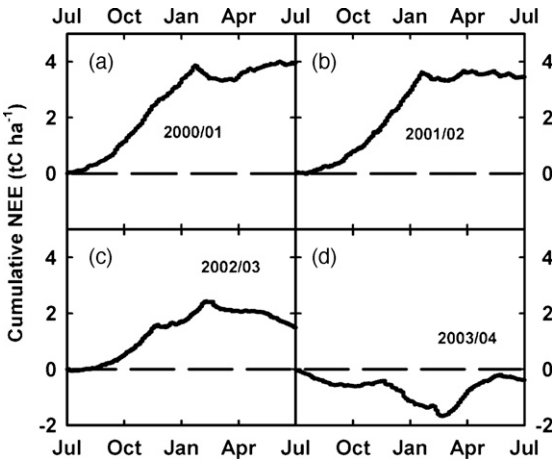

Fig. 12. Cumulative NEE in each of four years. Sums were initialised on 1 July in each year. Positive values designate carbon uptake. Final totals were 4.0, 3.5, 1.5 and −0.4 t C ha^{-1} $year^{-1}$ for each of the four years.

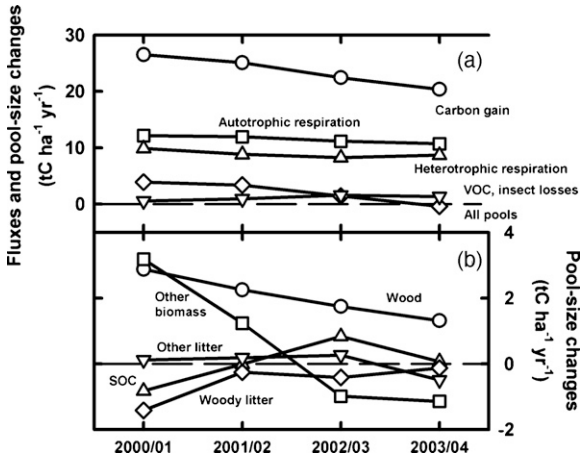

Fig. 13. Summary of the main fluxes in the system and change in the size of all pools (a) and details of changes in five key pools (b). 'VOC, insect losses' refers to carbon losses from volatile organic compounds and insect respiration. 'All pools' refers to carbon loss or gain through changes in the size of the sum total of all carbon pools in the system, with positive values indicating increasing pool sizes.

also strong within-year variation, with the strong carbon gain in 2000/2001 and 2001/2002, for example, being restricted to the first half of the year, whereas the system was close to carbon-neutral for the second half of the year. Similar extended periods of carbon gain or losses occurred in the other years as well.

A partitioning between the various factors contributing to the between-year variation showed that total photosynthetic carbon gain was highest in 2000/2001 but gradually declined to be almost 25% lower in 2003/2004. There was less change in total respiratory carbon losses between years (Fig. 13a), with autotrophic respiration reduced by only about 10% and heterotrophic respiration by about 15%. In addition, it was estimated that sizeable amounts of carbon were lost due to insect respiration in the final two years of the study plus an on-going small loss of volatile organic compounds.

Average values of photosynthetic carbon gain were high compared to values reported for temperate forests in Europe (Valentini et al., 2000), the USA (Hanson et al., 2004; Turner et al., 2005) and Japan (Saigusa et al., 2005), which may be related to the long growing season with generally favourable climatic conditions at our experimental site. The high carbon gain did not translate into high NEE, however (Figs. 11 and 12), as much of the fixed carbon was lost in autotrophic and heterotrophic respiration while little carbon accumulated in new wood and other biomass production (Fig. 13).

Over the first two years of the study, the model indicated that there was a significant net increment in wood and other biomass, whereas over the second two-year period, net wood increment was nearly halved, and other biomass pools actually decreased by more than 1 t C ha^{-1} year^{-1} (Fig. 13b). In the first two years, the increment in 'other' biomass mainly reflected on-going growth in branch biomass and coarse roots. Over the last two years, the branch pool decreased because more branch biomass was lost during turn-over than was produced in new growth, and substantial biomass was also lost from the foliage and fine-root pools (data not shown).

Soil organic carbon slightly increased over 2003/2004 because there was enhanced litter input for organic matter formation from increased leaf shedding due to insect damage. Coarse woody litter (including dead standing trees) was still decreasing after a large litter influx during harvesting operations in the 1980s (see Fig. 2). That long-term loss was almost halted in 2003/2004 due to increased fresh input from enhanced tree mortality.

While the changes in the trends in soil organic carbon over the respective years of the experimental period are readily explained in terms of the changes in input and output over those years, those variations were of a magnitude to be quantitatively important in terms of the overall net carbon exchange of the forest. At the same time, these changes were too small to be experimentally verifiable. It is therefore only possible to assess whether the modelled trends are internally consistent and sensible in terms of changes in the external driving variables over the short and longer term.

4.5. Causes of reduced NEE

Figs. 11 and 12 indicate that NEE was substantially reduced in 2003/2004 compared to the earlier years. This coincided with a period of significantly below-average rainfall, elevated temperature, lower relative humidity and observations of substantial insect damage. The model provided a tool to distinguish between these possible causes of reduced NEE by performing a number of simulations

(i) with the standard parameters and weather inputs that had provided the best fit to observations;
(ii) with insect damage excluded;
(iii) with increased soil depth so that the access to additional water ensured that plants experienced no water stress over the experimental period; and
(iv) with relative humidity held constant at the average value observed over the experimental period.

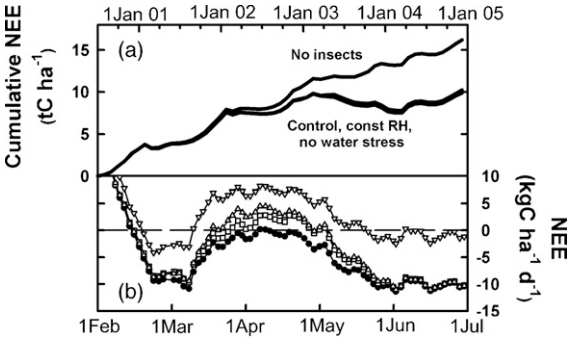

Fig. 14. Comparison of cumulative NEE over four years, with different stress factors excluded (a) and running 31-day means of NEE from February to July 2003, the period with greatest atmospheric and soil-water stress (b). Control conditions are shown as (●), no insect damage (▽), no water stress (△) and constant relative humidity (□).

The model comparison suggested that the reduced carbon gain was primarily due to insect damage, whereas elimination of soil water stress or keeping relative humidity constant had only very minor effects on calculated NEE (Fig. 14a). Over the experimental period, the most severely reduced soil-water deficits coupled with lower atmospheric humidity were experienced during the early months and into autumn of 2003. Over that period, the elimination of drought or changes to atmospheric humidity had some minor effect on improving the site carbon balance, but the effect of insect damage predominated even over that period (Fig. 14b).

Water stress was generally relatively unimportant at the experimental site because average annual rainfall considerably exceeds average annual tree water use. As the soils are fairly deep, they can hold large amounts of water that can be carried over from earlier periods with excess rainfall. As such, the site is quite unusual amongst Australian ecosystems (e.g. Roxburgh et al., 2004).

It is not known, however, why the insect outbreak was so severe over the experimental period, and it may be indirectly linked to water stress. Other stands in the vicinity of the experimental site also experienced significant tree mortality over that period, which was thought to be related to drought stress (H. Keith, unpublished). However, the model simulations indicated strongly that at our experimental site, water stress was not directly responsible for the large reduction in carbon gain over 2003/2004.

5. General discussion and conclusions

In the present work, we used a comprehensive ecosystem model to estimate net ecosystem exchange rates over time frames from days to decades. The model was constrained by a wide range of measurements obtained at the site and made use of the particular strengths of respective measurements techniques. The use of these multiple constraints provided the strongest possible overall constraint on the site carbon budget.

These measurements included eddy flux measurements of daytime carbon exchange, which allowed us to follow the time course of carbon exchange on a day-to-day and seasonal basis. We purposefully used only daytime values because we had high confidence in these values. We used direct soil respiration measurements as our primary method for estimating night-time carbon losses which we preferred over night-time eddy flux measurements because of measurement uncertainty during times of atmospheric stability in gently sloping terrain (Aubinet et al., 2003, 2005).

The technique for measuring soil respiration used in the present study (Keith and Wong, 2006) gave internally consistent results in that the seasonal pattern of soil respiration was well described by the temperature and moisture effects on soil respiration. The absolute magnitude of modelled rates was also strongly constrained by other observations in the system, especially litter fall rates as leaf litter was one of the primary sources of fresh substrate for subsequent heterotrophic respiration.

Eddy flux measurements also provided estimates of water loss from the site. As transpiration is closely coupled to photosynthetic carbon gain, it provided a further constraint on daytime carbon exchange rates. It also provided important constraints on the movement of water which affected the development of plant water stress and reduced soil respiration during times of soil and litter drying.

The model was further constrained by considerations of the conservation of carbon and nitrogen, with these elements either transferred between pools in defined ways or gained or lost from the system in accordance with well-defined processes, such as photosynthesis. In the case of nitrogen, total site nitrogen stocks were modelled to remain fairly constant over the growth and development of the stand. Previous work had shown that consideration of the nitrogen budget adds important constraints on carbon gains and losses from forest ecosystems (Kirschbaum et al., 2003).

The model was also constrained by general scientific understanding of ecophysiological processes, such as the three halves self-thinning law, the dependence of photosynthesis on temperature, light, water and nitrogen availability, the physical processes governing the evaporation of water and the temperature and moisture

dependence of organic matter decomposition. Consideration of all of these factors together constituted a further constraint on the overall site carbon budget.

The NEE estimates calculated here are substantially lower than NEE estimates reported in the earlier work of Leuning et al. (2005). Leuning et al. (2005) had been careful to avoid measurements on nights with stable atmospheric conditions and only used measurements obtained on nights with some turbulence, defined as nights with a friction velocity threshold above 0.25 m s^{-1}. These observations had then been expressed as a function of soil temperatures which was used for nights with missing data or when atmospheric conditions were too stable.

Such a method had been applied in many previous eddy flux studies (Goulden et al., 1996; Falge et al., 2001a,b) but still appeared to underestimate night-time respiration rates as discussed in detail by van Gorsel et al. (2007). As a consequence, NEE reported in Leuning et al. (2005) was slightly overestimated, especially for the low NEE years 2002–2003 and 2003–2004. It appears that the problems of night-time fluxes obtained with eddy flux technique can be largely overcome with the novel technique developed by van Gorsel et al. (2007) so that it provided very similar results as the full model integration for photosynthesis and net ecosystem exchange (Fig. 8).

It is a general concern, however, that estimates of annual NEE that rely on eddy flux measurements alone may overestimate NEE. This problem is widely acknowledged by the eddy flux community (e.g. Aubinet et al., 2003, 2005; Miller et al., 2004; Feigenwinter et al., 2004) who are investing substantial resources to develop alternative techniques such as those suggested by van Gorsel et al. (2007) or Gu et al. (2005).

A separate problem relates to the systematic problem of missing eddy flux measurements on rainy days (Fig. 7), which is likely to lead to an overestimation of net ecosystem exchange derived solely from eddy flux measurements. The magnitude of that problem depends on the number of missing data and to what extent the model assumptions of high soil respiration rates on such days are justified.

For carbon to be retained in the system (implying a positive NEE), it must have accumulated in one or more pools. Observations of changes in the size of such pools thereby provide one important constraint on possible estimates of NEE. In the present work, the observations of net stem-wood increment showed that only moderate amounts of carbon were accumulating in that pool. In principle, carbon could have accumulated in other biomass or litter pools or in soil organic matter. The long-term simulations provided constraints on the possible magnitude of pool-size changes over the experimental period which meant that they would be unlikely to have accumulated large amounts of carbon either.

When there were no major disturbances from either fire or insect-pest outbreaks, this particular forest system appeared to generally continue to accumulate carbon. On average, the site receives substantial more rain than annual evapotranspiration, and because of its relatively deep soil profile, the effect of water stress on constraining carbon uptake is likely to be limited. Even though the 2002 and 2003 seasons were exceptionally dry (Leuning et al., 2005), modelled NEE did not appear to be limited by water availability under even those conditions (Fig. 14), and it is unlikely to have been an important constraint over the life of this stand. This conclusion is likely to be different for the majority of Australian eucalypt forests for which water stress is likely to play a much more important role (Roxburgh et al., 2004).

Measured temperatures differed between years, but as neither extremely low nor extremely high temperatures are common at the experimental site, it is not expected that there are large enough year-to-year temperature variations to significantly affect the site's carbon balance. Vapour pressure differences can vary between years in line with differences in temperature, but this, too, appears to play only a minor role (Fig. 14).

A factor that appeared to play an important role over the experimental period, however, was insect damage (Fig. 14). Large unseasonal leaf-litter fall was observed in 2003 (Fig. 4). This tangible loss must have been preceded by leaf damage that reduced the photosynthetic capacity of leaves. Carbohydrate must have also been used for insect metabolism. Some of that carbon would have been lost through insect respiration and some of it embodied in insect bodies for later carbon loss upon the insects' death and decomposition.

An earlier episode of major insect damage was recorded for the period from 1955 to 1964, with estimated reductions in growth increment by 20–50% and recorded death in some years of up to 50% of trees (in 1960). There are no records of other episodes of insect damage, but insect damage is likely to cause a variable but on-going carbon drain from these forests. It leads to the important generic question of what particular factor determines the periodicity and severity of insect-pest outbreaks. It may be linked to the occurrence of drought. If that is the case then drought can have important indirect effects on stand productivity.

Overall, the study showed that an integrated approach to measuring a site carbon budget, based on multiple measurements and integrated through a comprehensive forest-growth model, can provide the strongest possible constraints on the site carbon budget. Once a site has been fully characterised, it then becomes possible to dissect its overall budget into the different components, such as separating total net fluxes between gains and losses, or separating losses between autotrophic and heterotrophic respiration. Such comprehensive studies can then become invaluable tools in understanding the factors responsible for modifying site carbon budgets in different years or under different conditions.

Acknowledgments

We would like to thank the Australian Greenhouse Office for providing funds to support this study, Jacqui England for provision of the fine-root data, Vijay Koul, Peter Leppert and John Smith for technical assistance with field and laboratory measurements, Phil Ryan for many useful insights into the main factors that determine stand properties and carbon exchange rates at Tumbarumba and two anonymous referees for many useful comments and suggestions on the manuscript. Dale Hughes, Steve Zegelin are acknowledged for maintaining the CSIRO flux tower. The experimental site is managed by Forests New South Wales, and we thank their staff for their wide-ranging support over many years.

Appendix A. Radiation calculations

The calculation of radiation follow the method outlined in Collares-Pereira and Rabl (1979) and Gates (1980). The effect of atmospheric turbidity was based on a routine modified from that originally given by Bristow and Campbell (1984) and Allen (1997). The procedure used here for calculating atmospheric absorption principally differs from that used previously by explicit inclusion of a precipitation term. Similar procedures for calculating daily solar radiation have also been given by Hamer (1999), Nödj and Hari (2001) and Yang et al. (2006).

Incident daily net radiation, Q_i, was calculated as:

$$Q_i = Q_0\{0.147 + 0.796[1 - \exp(-0.080\Delta T)]\} \times [0.657 + 0.343\exp(-0.293P)] \quad \text{(A1)}$$

where ΔT is the diurnal temperature range, P is precipitation and Q_0 is the radiation that would be received if there were no atmospheric turbidity absorbing part of incoming radiation.

The diurnal temperature range was calculated as:

$$\Delta T = T_{\max} - T_{\min(-1)} \quad \text{(A2)}$$

where $T_{\max}$ is daily maximum, $T_{\min(-1)}$ the minimum temperatures of the preceding night.

Incident radiation can be reduced by cloud cover. Clouds also reduce the diurnal temperature range and may bring precipitation. Information about precipitation and the diurnal temperature range can thus be used to infer the presence of clouds and their effect on reducing incident radiation. It was found that the minimum temperature of the night preceding the day of interest provided a stronger constraint on atmospheric turbidity than the minimum temperature of the following night.

The numeric parameters in Eq. (A1) were fitted to data from the Tumbarumba site in order to minimise the residual sums of squares of modelled minus observed data.

Q_0 was calculated as:

$$Q_0 = 86,400 Q_x d_{\text{sol}}^2 \sin\left(\frac{\pi L}{180}\right)\sin(\delta)\frac{[d_{\text{rel}} - \tan(d_{\text{rel}})]}{\pi} \quad \text{(A3)}$$

where Q_x is the incident daily radiation outside the Earth's atmosphere (1360 MJ m^{-2} day^{-1}), 86,400 the number of seconds in a day, d_{sol} is the relative distance between the sun and the Earth, d_{rel} is relative daylength in radians, L is latitude and δ is the solar declination.

The variation in the mean distance between sun and Earth was calculated based on information in Gates (1980) as:

$$d_{\text{sol}} = 1 + 0.01705\cos\left[\frac{2\pi(d-3)}{365.24}\right] \quad \text{(A4)}$$

where d is the day of the year.

Solar declination, δ, was calculated following Collares-Pereira and Rabl (1979) as:

$$\delta = \arcsin[0.3979\sin(\Gamma)] \quad \text{(A5)}$$

with Γ calculated as:

$$\Gamma = \frac{2\pi(d+284)}{365.24} \quad \text{(A6)}$$

Relative daylength (in radians), d_{rel}, was calculated as:

$$d_{\text{rel}} = 0 \quad \text{if } d_{\text{L}} \le -1 \quad \text{(A7a)}$$

$$d_{\text{rel}} = \pi \quad \text{if } d_{\text{L}} \ge 1 \quad \text{(A7b)}$$

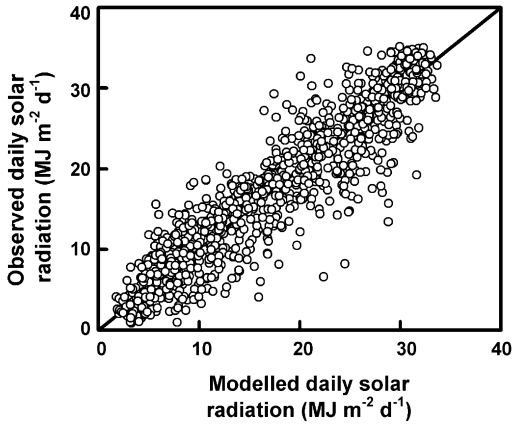

Fig. A1. Observed versus predicted incident radiation at the Tumbarumba site. EF = 0.850; O = 0.950M + 1.10 (r^2 = 0.854). The line is a 1:1 relationship.

$$d_{\mathrm{rel}} = \pi - \arccos(d_{\mathrm{L}}) \quad \text{if} \quad 1 < d_{\mathrm{L}} < 1 \tag{A7c}$$

with d_{L} calculated as:

$$d_{\mathrm{L}} = \tan(0.0174533L)\tan(\delta) \tag{A8}$$

A test of the radiation calculation routine against data from the Tumbarumba site is shown in Fig. A1. The parameters of best fit are given in Eq. (A1). Maximum incident radiation throughout the year ranged from 15.1 to 44.3 MJ m^{-2} day^{-1} without atmospheric turbidity. This seasonal pattern was well described by Eqs. (A3)–(A8).

Maximum observed actual radiation did not exceed 35.8 MJ m^{-2} day^{-1} on even the clearest days, and was reduced much more on cloudy days. The terms included in Eq. (A1) were able to explain a large part of that variation, with the diurnal temperature range being more important than rainfall in explaining variations in reductions in daily radiation. Overall, the equations were able to explain 85% of observed variation, with virtually no residual bias. Hence, the equations could be used with some confidence to calculate radiation for those days for which no measurements were available.

Appendix B. New calculation routines in CenW 3.1

B.1. Water relations

The detailed modelling of soil respiration and evaporation required a more detailed representation of the drying and wetting cycles in the litter and different soil layers than had been required for previous work. For the present work the whole profile was divided into a litter layer and six soil layers (0–5, 5–20, 20–40, 40–80, 80–200 and 200–430 cm), assumed to be able to hold 10, 30, 40, 60, 120 and 230 mm of plant available water, respectively.

The calculation of soil and litter evaporation was reformulated from a simpler version used previously, and the effect of a litter layer as both a contributor to evaporation, and in preventing soil evaporation, was explicitly, and dynamically, included. It was assumed that roots could not access water from the litter layer. Incoming rainfall wetted the litter layer first. If water in the litter layer was in excess of the layer's water-holding capacity, the excess percolated further down into the soil, from where it could be lost by evaporation or taken up by plants and lost in transpiration.

Evaporation from litter, E_{lit}, and the soil, E_{soil}, were calculated with the Penman-Monteith equation as:

$$E_{\mathrm{lit}} = h f_{\mathrm{lit}} \frac{(\sigma R_n + \Delta p_{\mathrm{a}} C_p / r_{\mathrm{a}})/(\sigma + \gamma(r_{\mathrm{a}} + r_{\mathrm{lit}})/r_{\mathrm{a}})}{L_h} \tag{B1a}$$

$$E_{\mathrm{soil}} = h(1 - f_{\mathrm{lit}}) \frac{(\sigma R_n + \Delta p_{\mathrm{a}} C_p / r_{\mathrm{a}})/(\sigma + \gamma(r_{\mathrm{a}} + r_{\mathrm{soil}})/r_{\mathrm{a}})}{L_h} \tag{B1b}$$

where h is day length (s), f_{lit} is the fraction of ground covered by litter, σ (Pa K^{-1}) is the derivative of the saturation vapour pressure with respect to temperature, R_n (J m^{-2} day^{-1}) is net radiation that passes through the canopy and reaches the ground, p_{a} (kg m^{-3}) the density of air, C_p (J kg^{-1} K^{-1}) the specific heat of air, Δ (Pa) the vapour pressure saturation deficit of the air, r_{a} (s m^{-1}) is aerodynamic resistance, γ (Pa K^{-1}) the psychrometric constant, L_h (J kg^{-1}) the latent heat of vaporisation and r_{lit} and r_{soil} (s m^{-1}) the diffusion resistances out of the litter and upper soil layers, respectively. Aerodynamic resistance in these calculations was taken to be five times as large as the user-input aerodynamic resistance for transpiration from the canopy (Massman, 1992; Kelliher et al., 1993).

The fraction of the surface of mineral soil covered by litter, f_{lit}, was calculated as:

$$f_{\mathrm{lit}} = 1 - \exp(-f_{\mathrm{mulch}} L_{\mathrm{s}}) \tag{B2}$$

where L_{s} is the amount of non-woody surface litter including partly decomposed material, and f_{mulch} an empirical parameter that describes the surface coverage by different litter types.

Diffusion resistances from the litter, r_{lit}, and soil layers, r_{soil}, were calculated, loosely following Camillo

and Gurney (1986), as:

$$r_{\mathrm{lit}} = \frac{800 W_{\mathrm{lit,max}}}{W_{\mathrm{lit}}} \tag{B3a}$$

$$r_{\mathrm{soil}} = \frac{800 W_{\mathrm{soil(1),max}}}{W_{\mathrm{soil(1)}}} \tag{B3b}$$

where W_{lit} and $W_{\mathrm{soil(1)}}$ are the amounts of water held in the litter and upper-most soil layers, respectively, and $W_{\mathrm{lit,max}}$ and $W_{\mathrm{soil(1),max}}$ are their maximum water-holding capacities, respectively.

In the case of the upper soil layer, $W_{\mathrm{soil(1),max}}$ was user-specified, whereas for the litter layer, maximum water-holding capacity was calculated as:

$$W_{\mathrm{lit.max}} = L_{\mathrm{s}} f_{\mathrm{hold}} \tag{B4}$$

where f_{hold} is a user-input parameter that gives the water holding capacity per unit of litter dry weight.

B.2. Moisture and temperature dependence of decomposition rates

For each layer, including the litter and each soil layer, decomposition rate, r_{p}, of each organic matter pool was calculated as:

$$r_{\mathrm{p}} = k_{\mathrm{p}} d_T d_{\mathrm{wat}} \tag{B5}$$

where k_{p} is a pool specific decomposition rate based on the parameters given by Parton et al. (1987), and d_T and d_{wat} are temperature and moisture modifiers, respectively.

The temperature modifier was described as:

$$d_T = \exp\left[\frac{3.36 T_{\mathrm{soil}} - 40}{T_{\mathrm{soil}} + 31.79}\right] \tag{B6}$$

where T_{soil} is soil temperature and the constants were derived from a literature survey of relevant temperature dependencies derived in different laboratory incubations (Kirschbaum, 2000).

The moisture effect on decomposition activity, d_{wat}, was calculated as:

$$d_{\mathrm{wat}} = d_{\mathrm{min}} + (1 - d_{\mathrm{min}})\left(\frac{W}{W_{\mathrm{lim}}}\right)^{\mathrm{w}} \tag{B7}$$

where d_{min} is the minimum decomposer activity that continued even under apparently dry conditions, W is the amount of water held in each layer, W_{lim} is an empirical factor that describes the limit of water content on restricting decomposer activity, and w is a further empirical term that describes the shape of the response of decomposer activity to water content. That derived term d_{wat} was then applied to the decomposer activity in each layer.

B.3. Plant respiration rate

Plant respiration rate was calculated for each plant organ, R_i, as:

$$R_i = R_{\mathrm{g},i} + R_{\mathrm{m},i} \tag{B8}$$

where $R_{\mathrm{g},i}$ is growth and $R_{\mathrm{m},i}$ maintenance respiration of tissue i.

Growth respiration was calculated as:

$$R_{\mathrm{g},i} = f_{\mathrm{g}} G_i \tag{B9}$$

where f_{g} is a parameter to express the respiratory carbon loss per unit of new growth, and G_i is new growth in each biomass compartment.

Maintenance respiration was calculated as:

$$R_{\mathrm{m}} = f_{\mathrm{m}} f_{\mathrm{t}} R_{\mathrm{b}} N_i \tag{B10}$$

where f_{m} is an empirical parameter that gives the respiration rate per unit of nitrogen, f_{t} is a temperature modifier, R_{b} a respiration rate base parameter and N_i is the amount of nitrogen in a biomass component. For foliage, only night-time respiration was included, with daytime respiration included in the calculations of daytime net photosynthesis.

The temperature response of maintenance respiration includes both a short-term response to temperature and an acclimation response that tends to negate the longer-term temperature response so that respiration rates are often observed to be almost invariant with temperature (Gifford, 1995; Atkin et al., 2005). Hence, modification of the base rate of respiration, together with a short-term temperature-response function gave adequate description of both short- and long-term respiration responses to temperature. The base rate was thus adjusted as:

$$\frac{\mathrm{d}R_{\mathrm{b}}}{\mathrm{d}t} = \frac{[(1/f_t) - R_{\mathrm{b}}]}{\tau_{\mathrm{r}}} \tag{B11}$$

where τ_{r} is the time constant for respiratory acclimation.

The temperature response was calculated as:

$$f_{\mathrm{t}} = \exp[\alpha + \beta T(2T_{\mathrm{max}} - T)] \tag{B12}$$

where T is daily mean temperature in °C, and T_{max} is the temperature of maximum respiration rate and β is a user-input parameter. T_{max} and β together determine the temperature dependence of respiration rate. The term α determines the absolute rate of the function which is set

to a value so that the function is normalised to '1' at 25 °C.

B.4. Insect damage

Sap sucking insects cause a diversion of photosynthate from trees to insects. For specified dates, this extra respiratory loss, R_p (via insect respiration) was simply calculated as:

$$R_p = k_{p,1} \tag{B13}$$

where $k_{p,1}$ is a user defined constant (in kgDW ha^{-1} day^{-1}). This extra respiratory carbon loss was added to other carbon losses and the amount of available carbohydrate for subsequent growth was reduced by the amount diverted to insect respiration.

Carbohydrate loss was accompanied by a loss of soluble nitrogen, N_{pest}, calculated as:

$$N_{pest} = \frac{k_{p,1} N_{sol}}{C_{sol}} \tag{B14}$$

where N_{sol} and C_{sol} are the amounts of carbon and nitrogen in the plant-internal soluble pools, respectively. It was assumed, however, that nitrogen extracted from the plant pool was not lost from the system but added to the surface litter (so that time delays due to the death of insects were ignored).

Insect pests also caused additional leaf senescence, S_p, also defined simply as:

$$S_p = k_{p,2} \tag{B15}$$

where $k_{p,2}$ is a user defined constant (in kg DW ha^{-1} day^{-1}) that gives the additional amount of foliage shed on each day as a result of the insect damage. This foliage loss reduced leaf area and added senesced foliage to the surface litter pool. It was assumed that no nitrogen retranslocation took place before leaves were shed due to insect damage.

Leaf necrosis and associated psyllid coatings also reduced photosynthetic carbon gain, with an effect on maximum photosynthetic capacity. Hence, maximum photosynthesis, A_{max}, was calculated as:

$$A_{max} = (1 - k_{p,3}) f(N, T_{damage}, W_{lim}, C_{lim}, T_{lim}) \tag{B16}$$

where $k_{p,3}$ is the reduction in photosynthetic capacity by insect damage and the second term states that it is calculated as a function of nitrogen status, temperature damage from previous days, water-stress and CO_2 limitation functions and a temperature modifier based on the current temperature. These functions have been defined in detail by Kirschbaum (1999).

The timing and parameters values of the three pest-damage parameters is given in Table C2 of Appendix C.

B.5. Emission of volatile organic compounds

A small fraction of carbon fixed in photosynthesis can be lost from the ecosystem in the emission of volatile organic compounds, especially isoprene (Guenther et al., 1995; He et al., 2000; Sharkey and Yeh, 2001). This is an important flux as the initial CO_2 uptake is recorded in eddy flux observations but the loss is not observed as a CO_2 flux, yet any loss reduces the system's net ecosystem exchange.

The carbon loss, V, was calculated simply as:

$$V = vA \tag{B17}$$

where A is the rate of stand-level photosynthesis and v is a simple proportionality term that links photosynthesis and the emission rate of volatile organic compounds.

Appendix C. Parameters used

Table C1 provides a list of key parameters used in the modelling. Parameters are either those that are used and described in the text or are given by Kirschbaum (1999) (Table C2).

Table C1
Key parameters used in the simulations

Parameter description	Value
Atmospheric N deposition (kg N ha^{-1} year^{-1})	2.0
Canopy aerodynamic resistance (s m^{-1})	25
Litter water-holding capacity (kg (kg DW)$^{-1}$)	2
Mulching effect, f_{mulch} (% (t DW)$^{-1}$ ha^{-1})	3
Foliage water holding capacity per unit leaf area index (for rainfall interception) (mm)	0.15
Soil water threshold for water stress	0.4
Water stress sensitivity of decomposition relative to plant processes, w	1
Decomposition activity under extremely dry conditions, d_{min}	0.2
Self-thinning parameter	14.96
Fine-root turn-over (year^{-1})	0.41
Branch turn-over (year^{-1})	0.06
Bark turn-over (year^{-1})	0.059
Specific leaf area (m^2 (kg DW)$^{-1}$)	5.0
Threshold N concentrations (N_0) (g N (kg DW)$^{-1}$)	10
Non-limiting N concentration (N_{sat}) (g N (kg DW)$^{-1}$)	14

Table C1 (*Continued*)

Parameter description	Value
Maximum assimilation rate (no limitations) (μmol m^{-2} s^{-1})	38
Ball–Berry stomatal parameter (unstressed)	9
Ball–Berry stomatal parameter (stressed)	5
Minimum temperature for photosynthesis (°C)	−6
Minimum temperature for optimum phs. (°C)	13
Maximum temperature for optimum phs. (°C)	30
Emission of volatile organic compounds, υ	0.02
Respiration rate per unit nitrogen	0.06
Temperature of maximum respiration rate (°C)	50
Temperature parameter in the response function of respiration rate (β)	0.4×10^{-3}
Time constant for acclimation of respiration (τ_r) (days)	35
Growth respiration (kg kg^{-1})	0.25
Age for halved productive potential (years)	58
exponential term in age function	4
Foliar lignin concentration (%)	20
Root lignin concentration (%)	30
Relative decomposability of branches (relative to structural litter)	1.5
Relative decomposability of stems (relative to structural litter)	5.0
Allometric relationship (weight = f(dbh, height))	2.358, 0
Allometric relationship height vs. dbh	0.853, 0.682
Fine root:foliage ratio (nitrogen-unstressed)	2.0
Fine root:foliage ratio (nitrogen-stressed)	4.0
Foliage:branch ratio	0.74
Stem:branch	0.73
Coarse roots:stem wood	0.23
Bark:stem wood	0.34
Allocation to seed and seed capsules	0.075
Allocation to pollen	0.075
Minimum wood allocation	0.21

Table C2
Parameters to describe insect damage

Day	Month	Year	Sap sucked, $k_{p,1}$ (kg DW ha^{-1} day^{-1})	Senescence, $k_{p,2}$ (kg DW ha^{-1} day^{-1})	Reduced phs., $k_{p,3}$ (%)
1	7	2001	1	0	2.5
1	7	2002	2	0	10
1	3	2003	5	0	20
11	4	2003	5	4.5	20
11	5	2003	5	5.5	20
10	6	2003	5	1	20
1	10	2003	5	0	20
1	1	2004	0	0	0

References

Allen, R., 1997. Self-calibrating method for estimating solar radiation from air temperature. J. Hydrol. Eng. 2, 56–67.

Atkin, O.K., Bruhn, D., Hurry, V.M., Tjoelker, M.G., 2005. The hot and the cold: unravelling the variable response of plant respiration to temperature Funct. Plant Biol. 32, 87–105.

Aubinet, M., Heinesch, B., Yernaux, M., 2003. Horizontal and vertical CO_2 advection in a sloping forest. Bound.-Layer Meteorol. 108, 397–417.

Aubinet, M., Berbigier, P., Bernhofer, C.H., Cescatti, A., Feigenwinter, C., Granier, A., Grunwald, T.H., Havrankova, K., Heinesch, B., Longdoz, B., Marcolla, B., Montagnani, L., Sedlak, P., 2005. Comparing CO_2 storage and advection conditions at night at different Carboeuroflux sites. Bound.-Layer Meteorol. 116, 63–94.

Baldocchi, D.D., 2003. Assessing the eddy covariance technique for evaluating carbon dioxide exchange rates of ecosystems: past, present and future. Global Change Biol. 9, 479–492.

Baldocchi, D.D., Wilson, K.B., 2001. Modeling CO_2 and water vapour exchange of a temperate broadleaved forest across hourly to decadal time scales. Ecol. Model. 142, 155–184.

Ball, J.T., Woodrow, I.E., Berry, J.A., 1987. A model predicting stomatal conductance and its contribution to the control of photosynthesis under different environmental conditions. In: Biggins, J. (Ed.), Progress in Photosynthesis Research, vol. IV. Martinus Nijhoff, Dordrecht, pp. 221–224.

Bristow, K.L., Campbell, G.S., 1984. On the relationship between incoming solar radiation and daily maximum and minimum temperature. Agric. For. Meteorol. 31, 159–166.

Camillo, P.J., Gurney, R.J., 1986. A resistance parameter for bare-soil evaporation models. Soil Sci. 141, 95–105.

Collares-Pereira, M., Rabl, A., 1979. The average distribution of solar radiation – correlation between diffuse and hemispherical and between daily and hourly insolation values. Solar Energy 22, 155–164.

Curtis, P.S., Hanson, P.J., Bolstad, P., Barford, C., Randolph, J.C., Schmid, H.P., Wilson, K.B., 2002. Biometric and eddy-covariance based estimates of annual carbon storage in five eastern North American deciduous forests. Agric. For. Meteorol. 113, 3–19.

Falge, E., Baldocchi, D., Olson, R., Anthoni, P., Aubinet, M., Bernhofer, C., Burba, G., Ceulemans, G., Clement, R., Dolman, H., Granier, A., Gross, P., Grunwald, T., Hollinger, D., Jensen, N.O., Katul, G., Keronen, P., Kowalski, A., Lai, C.T., Law, B.E., Meyers, T., Moncrieff, J., Moors, E., Munger, J.W., Pilegaard, K., Rannik, U., Rebmann, C., Suyker, A., Tenhunen, J., Tu, K., Verma, S., Vesala, T., Wilson, K., Wofsy, S., 2001a. Gap filling strategies for long term energy flux data sets. Agric. For. Meteorol. 107, 71–77.

Falge, E., Baldocchi, D.D., Olson, R., Anthoni, P., Aubinet, M., Bernhofer, Ch., Burba, G., Ceulemans, R., Clement, R., Dolman, H., Granier, A., Gross, P., Grünwald, T., Hollinger, D., Jensen, N.-O., Katul, G., Keronen, P., Kowalski, A., Lai, C.T., Law, B.E., Meyers, T., Moncrieff, J., Moors, E., Munger, J.W., Pilegaard, K., Rannik, Ü., Rebmann, C., Suyker, A., Tenhunen, J., Tu, K., Verma, S., Vesala, T., Wilson, K., Wofsy, S., 2001b. Gap filling strategies for defensible annual sums of net ecosystem exchange. Agric. For. Meteorol. 107, 43–69.

Farrow, R.A., 1996. Insect pests of eucalypts on farmland and in plantations in southeastern Australia. CSIRO Identification Leaflets, CSIRO, Melbourne, 60 pp.

Farquhar, G.D., von Caemmerer, S., 1982. Modelling of photosynthetic response to environmental conditions. In: Lange, O.L., Nobel, P.S., Osmond, C.B., Ziegler, H. (Eds.), Physiological Plant Ecology II. Water Relations and Carbon Assimilation, Encyclopedia of Plant Physiology, New Series, vol. 12 B. Springer-Verlag, Berlin, Heidelberg, New York, pp. 549–588.

Feigenwinter, C., Bernhofer, C.H., Vogt, R., 2004. The influence of advection on the short term CO_2 budget in and above a forest canopy. Bound.-Layer Meteorol. 113, 201–224.

Finnigan, J.J., Clement, R., Malhi, Y., Leuning, R., Cleugh, H.A., 2003. A re-evaluation of long-term flux measurement techniques. Part I. Averaging and coordinate rotation. Bound.-Layer Meteorol. 107, 1–48.

Gates, D.M., 1980. Biophysical Ecology. Springer Verlag, New York, Heidelberg and Berlin, 611 pp.

Gifford, R.M., 1995. Whole plant respiration and photosynthesis of wheat under increased CO_2 concentration and temperature: long-term vs. short-term distinctions for modelling. Global Change Biol. 1, 385–396.

Goulden, M.L., Munger, J.W., Fan, S.-M., Daube, B.C., Wofsy, S.C., 1996. Measurements of carbon sequestration by long-term eddy covariance: methods, and a critical evaluation of accuracy. Global Change Biol. 2, 169–182.

Gu, L., Falge, E.M., Boden, T., Baldocchi, D.D., Black, T.A., Saleska, S.R., Suni, T., Verma, S.B., Vesala, T., Wofsy, S.C., Xu, L., 2005. Objective threshold determination for nighttime eddy flux filtering. Agric. For. Meteorol. 128, 179–197.

Guenther, A., Hewitt, C.N., Erickson, D., Fall, R., Geron, C., Graedel, T., Harley, P., Klinger, L., Lerdau, M., CcKay, W.A., Pierce, T., Scholes, B., Steinbrecher, R., Tallamraju, R., Taylor, J., Zimmerman, P., 1995. A global-model of natural volatile organic-compound emissions. J. Geophys. Res. 100, 8873–8892.

Hamer, P.J.C., 1999. An algorithm to provide UK global radiation for use with models. Comput. Electron. Agric. 22, 41–49.

Hanson, P.J., Amthor, J.S., Wullschleger, S.D., Wilson, K.B., Grant, R.F., Hartley, A., Hui, D., Hunt, E.R., Johnson, D.W., Kimball, J.S., King, A.W., Luo, Y., McNulty, S.G., Sun, G., Thornton, P.E., Wang, S., Williams, M., Baldocchi, D.D., Cushman, R.M., 2004. Oak forest carbon and water simulations: model intercomparisons and evaluations against independent data. Ecol. Monogr. 74, 443–489.

He, C.R., Murray, F., Lyons, T., 2000. Monoterpene and isoprene emissions from 15 Eucalyptus species in Australia. Atmos. Environ. 34, 645–655.

Keith, H., Jacobsen, K.L., Raison, R.J., 1997. Effects of soil phosphorus availability, temperature and moisture on soil respiration in *Eucalyptus pauciflora* forest. Plant Soil 190, 127–141.

Keith, H., Leuning, R., Cleugh, H.A., Jacobsen, K.L., 2005. Dramatic decline in net ecosystem carbon exchange in native forest due to drought and insect attack. In: Greenhouse 2005: Action on Climate Change Conference Proceedings, Melbourne, Australia, p. 60.

Keith, H., Wong, S.C., 2006. Measurement of soil CO_2 efflux using soda lime absorption: both quantitative and reliable. Soil Biol. Biochem. 38, 1121–1131.

Kelliher, F.M., Leuning, R., Schulze, E.-D., 1993. Evaporation and canopy characteristics of coniferous forests and grasslands. Oecologia 95, 153–163.

Kirschbaum, M.U.F., 1999. CenW, a forest growth model with linked carbon, energy, nutrient and water cycles. Ecol. Mod. 118, 17–59.

Kirschbaum, M.U.F., 2000. Will changes in soil organic matter act as a positive or negative feedback on global warming? Biogeochemistry 48, 21–51.

Kirschbaum, M.U.F., 2004. Direct and indirect climate-change effects on photosynthesis. Plant Biol. 6, 242–253.

Kirschbaum, M.U.F., 2005. A modeling analysis of the interactions between forest age and forest responsiveness to increasing CO_2 concentration. Tree Physiol. 25, 953–963.

Kirschbaum, M.U.F., Paul, K.I., 2002. Modelling carbon and nitrogen dynamics in forest soils with a modified version of the CENTURY model. Soil Biol. Biochem. 34, 341–354.

Kirschbaum, M.U.F., Simioni, G., Medlyn, B.E., McMurtrie, R.E., 2003. On the importance of including soil nutrient feed-back effects for predicting ecosystem carbon exchange. Funct. Plant Biol. 30, 223–237.

Leuning, R., Cleugh, H.A., Zegelin, S., Hughes, D., 2005. Carbon and water fluxes over a temperate *Eucalyptus* forest and a tropical wet/dry savanna in Australia: measurements and comparison with MODIS remote sensing estimates. Agric. For. Meteorol. 129, 151–173.

Massman, W.J., 1992. A surface energy balance method for partitioning evapotranspiration data into plant and soil components for a surface with partial canopy cover. Water Resour. Res. 28, 1723–1732.

Medlyn, B.E., Berbigier, P., Clement, R., Grelle, A., Loustau, D., Linder, S., Wingate, L., Jarvis, P.G., Sigurdsson, B.D., McMurtrie, R.E., 2005. Carbon balance of coniferous forests growing in contrasting climates: model-based analysis. Agric. For. Meteorol. 131, 97–124.

McKenzie, N.J., Ryan, P.J., 1999. Spatial prediction of soil properties using environmental correlation. Geoderma 89, 67–94.

Miller, S.D., Goulden, M.L., Menton, M.C., da Rocha, H.R., de Freitas, H.C., Figueira, A.M.S., de Sousa, C.A.D., 2004. Biometric and micrometeorological measurements of tropical forest carbon balance. Ecol. Appl. 14, 114–126.

Nash, J.E., Sutcliffe, J.V., 1970. River flow forecasting through conceptual models. 1. A discussion of principles. J. Hydrol. 10, 282–290.

Nödj, P., Hari, P., 2001. Instantaneous PAR estimated using long records of daily temperature and rainfall. Agric. For. Meteorol. 109, 47–59.

Oliver, C.D., Larson, B.C., 1990. Forest Stand Dynamics. McGraw-Hill, New York, 467 pp.

Parton, W.J., Schimel, D.S., Cole, C.V., Ojima, D.S., 1987. Analysis of factors controlling soil organic matter levels in Great Plains grasslands. Soil Sci. Soc. Am. J. 51, 1173–1179.

Pretzsch, H., 2002. A unified law of spatial allometry for woody and herbaceous plants. Plant Biol. 4, 159–166.

Roxburgh, S.H., Barrett, D.J., Berry, S.L., Carter, J.O., Davies, I.D., Gifford, R.M., Kirschbaum, M.U.F., McBeth, B.P., Noble, I.R., Parton, W.G., Raupach, M.R., Roderick, M.L., 2004. A critical overview of model estimates of net primary productivity for the Australian continent. Funct. Plant Biol. 31, 1043–1059.

Running, S.W., Baldocchi, D.D., Turner, D.P., Gower, S.T., Bakwin, P.S., Hibbard, K.A., 1999. A global terrestrial monitoring network integrating tower fluxes, flask sampling, ecosystem modelling and EOS satellite data. Remote Sens. Environ. 70, 108–127.

Saigusa, N., Yamamoto, S., Murayama, S., Kondo, H., 2005. Interannual variability of carbon budget components in an AsiaFlux forest site estimated by long-term flux measurements. Agric. For. Meteorol. 134, 4–16.

Sands, P.J., 1995. Modelling canopy production. II. From single-leaf photosynthesis parameters to daily canopy photosynthesis. Aust. J. Plant Physiol. 22, 603–614.

Schelhaas, M.J., Nabuurs, G.J., Jans, W., Moors, E., Sabate, S., Daamen, W.P., 2004. Closing the carbon budget of a Scots pine forests in the Netherlands. Clim. Change 67, 309–328.

Sharkey, T.D., Yeh, S.S., 2001. Isoprene emission from plants. Annu. Rev. Plant Physiol. Plant Mol. Biol. 52, 407–436.

Soares, P., Tomé, M., Skovsgaard, J.P., Vanclay, J.K., 1995. Evaluating a growth model for forest management using continuous forest inventory data. For. Ecol. Manage. 71, 251–265.

Tang, J.W., Misson, L., Gershenson, A., Cheng, W.X., Goldstein, A.H., 2005. Continuous measurements of soil respiration with and without roots in a ponderosa pine plantation in the Sierra Nevada Mountains. Agric. For. Meteorol. 132, 212–227.

Turner, D.P., Ritts, W.D., Cohen, W.B., Maeirsperger, T.K., Gower, S.T., Kirschbaum, A.A., Running, S.W., Zhao, M., Wofsy, S.C., Dunn, A.L., Law, B.E., Campbell, J.L., Oechel, W.C., Kwon, H.J., Meyers, T.P., Small, E.E., Kurc, S.A., Gamon, J.A., 2005. Site-level evaluation of satellite-based global terrestrial gross primary production and net primary production monitoring. Global Change Biol. 11, 666–684.

Valentini, R., Matteucci, G., Dolman, A.J., Schulze, E.-D., Rebmann, C., Moors, E.J., Granier, A., Gross, P., Jensen, N.O., Pilegaard, K., Lindroth, A., Grelle, A., Bernhofer, C., Grünwald, T., Aubinet, M., Ceulemans, R., Kowalski, A.S., Vesala, T., Rannik, Ü., Berbigier, P., Loustau, D., Guomundsson, J., Thorgeirsson, H., Ibrom, A., Morgenstern, K., Clement, R., Moncrieff, J., Montagnani, L., Minerbi, S., Jarvis, P.G., 2000. Respiration as the main determinant of carbon balance in European forests. Nature 404, 861–865.

van Gorsel, E., Leuning, R., Cleugh, H.A., Keith, H., Suni, T., 2007. Nocturnal carbon efflux: reconciliation of eddy covariance and chamber measurements using an alternative to the u^*-threshold filtering technique. TellusB, doi:10.1111/j.1600-0889.2007.00252.x.

Wang, K.-Y., Kellomäki, S., Zha, T.S., Peltola, H., 2004. Component carbon fluxes and their contribution to ecosystem carbon exchange in a pine forest: an assessment based on eddy covariance measurements and an integrated model. Tree Physiol. 24, 19–34.

Yang, K., Koike, T., Ye, B., 2006. Improving estimation of hourly, daily, and monthly solar radiation by importing global data sets. Agric. For. Meteorol. 137, 43–55.